https://doi.org/10.1016/j.compositesb.2020.108149

ADVANCED STRESS-STRAIN MODEL FOR FRP-CONFINED CONCRETE IN SQUARE COLUMNS

G. Lin[1] and J.G. Teng[2*]

ABSTRACT

Extensive research has been conducted on the behavior of fiber reinforced polymer (FRP)-confined concrete in both circular and rectangular concrete columns. In the former columns, the stress-strain behavior of FRP-confined concrete is now well understood and can be closely predicted, but the same cannot be said about rectangular columns. This paper presents a new attempt at understanding and modeling the confinement mechanism in square columns as a special case of rectangular columns, leading to a new stress-strain model. The salient features of the new model include a more rigorous definition of the effective confinement area and a corner hoop strain-axial strain relationship based on advanced finite element results as well as a more reliable definition of the ultimate condition. The proposed model is analogous in approach to analysis-oriented stress-strain models for FRP-confined concrete in circular columns and represents a more advanced and robust method for modeling the stress-strain behavior of FRP-confined concrete in square columns than the existing empirically-based stress-strain models. The approach is also easily extendable to FRP-confined concrete in rectangular columns. The proposed model is shown to be accurate and perform better than the existing stress-strain models of the same type in predicting existing test results.

KEYWORDS

Fiber reinforced polymer (FRP); square columns; stress-strain models; stress distributions; finite element (FE) analysis.

1. INTRODUCTION

Strengthening of existing reinforced concrete (RC) columns using fiber reinforced polymer (FRP) confining jackets has now become a widely accepted technique in practice [1-5]. The behavior of FRP-confined concrete in RC columns has been extensively studied over the past two decades, leading to a significant number of stress-strain models. In particular, the response of FRP-confined concrete in circular columns is now well understood and can be closely predicted by some of the existing stress-strain models (e.g. [3, 6-10]). By contrast, much less is known about the behavior of FRP-confined concrete in square or rectangular columns even though these columns are more commonly found in practice [5, 11-23].

In an FRP-confined circular concrete column subjected to axial compression, the concrete is (nominally) uniformly confined by the FRP jacket. However, in an FRP-confined rectangular column, the confinement is non-uniform over the cross-section and only part of the section is

[1] Research Assistant Professor, Department of Civil and Environmental Engineering, The Hong Kong Polytechnic University, Hong Kong, China. Email: guanlin@polyu.edu.hk
[2] Chair Professor of Structural Engineering, Department of Civil and Environmental Engineering, The Hong Kong Polytechnic University, Hong Kong, China (* Corresponding author). Email: cejgteng@polyu.edu.hk

effectively confined [11, 18, 24-29]. The FRP confinement effectiveness is much reduced due to the flat sides and the sharp corners of the rectangular section, even after the rounding of the corners as is generally recommended. Corner rounding is needed both to enhance the confinement effectiveness and to reduce the detrimental effect of stress concentration at the corners. Because of the small flexural rigidity of the FRP jacket, the concrete in contact the flat sides of the column section receives the smallest confinement, while the concrete at the four corners receives the largest confinement [18, 25, 30-34]. Despite the much larger confining pressures acting on the corner concrete, the hoop tensile strains of the FRP jacket around the corners are lower than those along the flat sides; nevertheless, FRP rupture typically occurs near one of the rounded corners [5, 14, 33, 35].

Many researchers have employed a "shape factor" to reflect the difference in confinement between a circular column and a rectangular column. Existing stress-strain models for FRP-confined concrete in square columns, including both design-oriented stress-strain models (e.g. [11, 19, 24, 36-38]) and analysis-oriented stress-strain models (e.g. [31, 39]) have generally adopted this concept. This "shape factor" concept was originally proposed by Mander et al. [40] for confined concrete in rectangular RC columns with transverse steel reinforcement. The "shape factor" is usually defined as a function of the ratio of the effective-confinement area and the total cross-sectional area of concrete. The form of the effective-confinement area, however, has never been theoretically investigated, and its relationship to the actual stress distribution over the section is not at all clear. Moreover, as revealed in some finite element (FE) analyses, even within this effective-confinement area, the confining pressure and the axial stress distribution are rather non-uniform [18, 30, 32, 33, 41, 42]. The FRP confinement to the concrete near the flat sides of the rectangular section will be mobilized to be significant when the dilation of concrete is large enough [32]. Some researchers (e.g. [31, 39]) assumed that only the concrete within the effective-confinement area receives confinement from the FRP while the rest of the concrete (i.e., concrete near the flat sides) is unconfined, which obviously over-simplifies the complicated stress distribution of an FRP-confined rectangular section.

This paper presents a new attempt at understanding and modeling the stress-strain behavior of FRP-confined concrete in square columns as a special case of rectangular columns. Reliable and advanced FE simulations were conducted to gain an in-depth understanding of the confinement mechanism and to produce results that are then combined with experimental data to formulate a new stress-strain model. This stress-strain model is analogous to an analysis-oriented stress-strain model for FRP-confined concrete in circular columns (e.g. [6]). While the present study is limited to FRP-confined concrete in square columns, the same methodology can be readily extended to rectangular columns or perhaps other non-circular columns. The proposed model is shown to be accurate and perform better than the existing stress-strain models of the same type in predicting existing test results.

2. FINITE ELEMENT SIMULATIONS

A three-dimensional (3D) FE approach was employed to simulate the behavior of FRP-confined concrete in square columns under axial compression. In the FE simulation, only a thin slice of a quarter of an FRP-confined square section consisting of a single layer of elements was modeled (Figure 1). The concrete and the FRP jacket were represented using 8-node solid elements (C3D8R) and 4-node membrane elements (M3D4R), respectively, in ABAQUS (2011) [43]. Due to the small flexural rigidity of the FRP jacket, the two approaches of modelling the FRP jacket, using membrane elements (M3D4R) and shell elements (S4R) respectively, were found to provide almost identical predictions for the axial stress-axial strain response of confined concrete; however, the former elements allow the convergence of analysis to be achieved much more easily. Perfect bonding (i.e., no slips) between the FRP jacket and the concrete was assumed, which was achieved by means of the "Tie Option" in ABAQUS. Loading was applied by imposing axial displacements uniformly to the top nodes of the section.

The plastic-damage model developed by Yu et al. [44] and later modified slightly by Teng et al. [45] was employed to depict the three-dimensional constitutive behavior of FRP-confined concrete in square columns. Yu et al.'s model [44] was the first reliable constitutive model for FRP-confined concrete under both uniform confinement (e.g., FRP-confined concrete in circular columns) and non-uniform confinement (e.g., FRP-confined concrete in rectangular columns). The success of Yu et al.'s model [44] lies in relating the damage parameter, the hardening/softening rule, and the flow rule to the confinement state and relating the yield criterion to the third deviatoric stress invariant. This constitutive model has been successfully employed to predict responses of FRP-confined circular and square concrete columns under axial compression, hybrid FRP-concrete-steel double-skin tubular columns [44], as well as FRP-confined RC columns under eccentric axial compression [8, 46]. Yu et al.'s model [44] has also been used by many other researchers (e.g. [33, 47]). The reader is referred to Yu et al. [44, 48] for more details of the constitutive model. Note that Yu et al. [44] proposed two methods (i.e., Method I and Method II) to evaluate the confinement stiffness ratio (i.e., the ratio between the effective confining pressure and the lateral strain) for non-uniformly confined concrete. Compared to Method I, Method II is more reasonable as it takes into account the non-uniformity of flow rule over a non-circular section [44] and thus was adopted in the FE modeling of the present study.

The FRP jacket had fibers only in the column hoop direction (i.e., around the perimeter of the column section) to provide confinement to the concrete. Therefore, an orthotropic linear-elastic-brittle material was assumed for the FRP jacket and a very small value (0.001 GPa) was adopted for the elastic modulus of the FRP jacket in the axial direction. A mesh convergence study was carried out, leading to an element size of around 5.0 mm for both the concrete and the FRP jacket. A more refined mesh (e.g., 2.5 mm) produced an average axial stress-axial strain curve of the confined concrete that is almost identical to the one with an element size of 5.0 mm [8, 46].

3. TYPICAL FE RESULTS

3.1. Axial Stress Distribution

It is well known that the concrete in a rectangular column is non-uniformly confined by the FRP jacket. The two lateral stress components acting on the concrete along the two axes of symmetry of the section vary significantly over the section, and one of the components may be much larger than the other depending on the location. Some researchers attempted to establish approximate distributions of the lateral confining stresses over the column section. On the basis of these distributions of lateral stresses, as well as a failure criterion for confined concrete, the axial stress distribution can be evaluated (e.g. [41]). However, it has been found that the complication in trying to predict accurately the confining stress distributions can be hardly justified by the accuracy of the method to evaluate the axial response of the column. In Nisticò and Monti's method [41], regression analysis of test results still needs to be carried out in order to achieve accurate predictions for the axial response. As a result, in the present study, the distribution of axial stress instead of that of either of the lateral confining stress components over the square section is treated in detail.

Figure 2 shows the axial stress distributions over a typical FRP-confined square section (referred to as the reference section hereafter) at three different loading levels (or deformation states) predicted by the FE model. The reference section had a sectional width of 150 mm with a corner radius of 25 mm confined by a two-ply carbon FRP (CFRP) jacket (hoop elastic modulus E_f = 250 GPa, thickness t_f = 0.33 mm). The compressive strength of unconfined concrete (f'_{co}) was 45 MPa. State C corresponds to an FRP hoop strain of 1.0% (which may be taken as a typical CFRP rupture strain in a rectangular column) at the centers of the rounded corners (i.e., the mid-arc points of the circular corners). This hoop strain at the corner centers (referred to as the corner center hoop strain ε_h hereafter) is taken as the key reference value as laboratory tests have shown that FRP-confined rectangular concrete columns generally fail by sudden rupture of the FRP jacket at or near one of the corners (often at one of the curvature change points between the rounded corners and their adjacent flat sides) [4, 35, 49, 50]. Figure 2 shows that, at an early deformation state (State A), the axial stress is uniformly distributed over the section; as the axial deformation increases, the axial stress distribution becomes increasingly more non-uniform (States B and C). More specifically, the axial stresses in the four corner regions become much larger than those away from the corners; that is, the FRP jacket provides much more effective confinement to the concrete in the corner regions than elsewhere. Along the flat sides of the section, the axial stresses are the lowest indicating that the confinement provided by the FRP jacket is the weakest here because of the small flexural stiffness of the FRP jacket.

In the contour plots of axial stress distribution at the three deformation states in Figure 3, the thick red curves represent an axial stress of 45 MPa, which is equal to the unconfined concrete strength. The concrete enclosed by the red curves has an axial stress larger than 45 MPa, so the enclosed region(s) may be taken as the region(s) with effective FRP confinement. It can be seen that the size and shape of the region(s) vary as the axial deformation increases; more specifically, the total area of effective confinement increases with the axial deformation. The definition of a constant effective-confinement area for the full range of stress-strain behavior as adopted in most of the existing stress-strain models thus needs some careful considerations. Figure 4 shows the lateral deformation (i.e., dilation) of FRP-confined concrete in the square section at State C. It is obvious that the dilation is the largest at the centers (mid-width locations) of flat sides and smallest at the centers of corners in the diagonal direction, indicating the smallest and the largest levels of FRP confinement at the two locations, respectively. Figures 5(a) and 5(b) show the magnitudes and directions of the two lateral principal stresses (σ_{max} and σ_{mid}) over the square section at Stage C, and Figure 5(c) shows the distribution of the $\sigma_{max}/\sigma_{mid}$ ratio over the entire square section. It is evident that the two lateral principal stresses are not equal due to the non-uniform FRP confinement over the section and the ratio between them varies over the section. It can be seen from Figure 5(c) that the concrete near the center of the square section is under relatively uniform confinement (with $\sigma_{max}/\sigma_{mid}$ ratios being close to 1.0). The two lateral principal stresses of the concrete at the centers of the four corners differ significantly with the maximum ratio being around 0.5, although the concrete there has the largest axial stress (see Figure 2). The concrete near the mid-width locations of flat sides has the lowest $\sigma_{max}/\sigma_{mid}$ ratios (close to 0), indicating that the concrete there is subjected to the highest non-uniformity of confinement.

3.2. Effective-Confinement Area

In order to obtain a reliable definition of the effective-confinement area which is suitable for the development of the full-range stress-strain response of FRP-confined concrete in a square column, four patterns of section division of a square section are proposed herein as shown in Figure 6. These patterns were proposed based on the axial stress distribution identified in the FE results of the present study (Figure 2). The first three patterns consist of two diagonal regions as well as four triangular regions near the four flat sides (Figure 6). As high stresses exist in the corner regions and also in the central region, the corner regions and the central region are separated from the diagonal regions in patterns (2) and (3), respectively, as shown in Figure 6. Pattern (4) consists of a circular central region and four corner regions to reflect the large difference in axial stress between the central region and the corner regions (see Figures 2b and 2c). It should be noted that, in the present study, the section is divided using straight lines for simplicity for the first three patterns since the use of more complex division lines at the cost of efficiency may not improve the accuracy of prediction significantly.

In addition to the definition of stress regions, two equivalent circular sections are defined (Figure 7). The first equivalent circular section has a perimeter that circumscribes the square section with rounded corners, while the second one has the same radius as that of the rounded corners. The first equivalent circular section has also been used by Lee et al. [31] for the calculation of the effective confining pressure in an FRP-confined square section; this equivalent circular section allows a smooth transition from a square section to a circular section (i.e., the equivalent circular section becomes the circular section itself when the corner radius becomes equal to half the section width). A slightly different equivalent circular section has previously been used by Lam and Teng [11] for the same purpose, which, however, does not allow a smooth transition between a square section and a circular section. The second equivalent circular section is proposed in the present study to reflect the state of confinement in the corner regions.

4. STRESS RATIOS

In order to predict the full-range stress-strain response of a square section, it is proposed herein that the stress-strain responses of the two equivalent circular sections be determined first and these responses are then related to the responses of different regions of the square section for a given section pattern (Figure 56). For this purpose, the average stress of each region of a given section pattern was extracted from the FE results of the reference section and the obtained average stress was compared with the axial stresses of the two equivalent circular sections (σ_{c1} and σ_{c2}). σ_{c1} and σ_{c2} were calculated using the analysis-oriented stress-strain model of Jiang and Teng [6] for a given hoop (or lateral) strain equal to the corner center hoop strain (ε_h) of the rounded square column from the FE analysis. Figure 2(c) illustrates the average axial stresses of the two regions in section Pattern (1) (σ_1 and σ_2) compared with the actual axial stress distribution.

The stress ratio results throughout the loading process for the four section patterns are shown in Figure 8. For section Pattern (1), it is seen that the average stress of Region 1 (σ_1) is very close to the stress of the first equivalent circular section (σ_{c1}) after ε_h exceeds approximately 0.002. For Region 2, σ_2 decreases during the later stage of loading, indicating that the concrete near the flat sides is not effectively confined by the FRP jacket. Nonetheless, it is found that the non-dimensional parameter β ($=\sigma_2/\sigma_{c1}-\sigma_2/\sigma_{c2}$) remains almost constant during the later stage, which means that the two curves of σ_2/σ_{c1} and σ_2/σ_{c2} are almost parallel to each other during the later stage [Figure 8(a)]. In section Pattern (2), the corner regions are separated from Region 1 of section Pattern (1). It is observed that the average axial stress of the corner regions (σ_3) in section Pattern (2) is always larger than σ_{c1}, but smaller than σ_{c2}, and the ratios of σ_3/σ_{c1} and σ_3/σ_{c2} do not remain constant during the full loading process. The average axial stress of Region 1 (σ_1) is also very close to σ_{c1}, although σ_1 becomes slightly smaller than σ_{c1} during the later loading stage due to the exclusion of the corner regions with large axial stresses [Figure 8(b)]. In section Pattern (3), the central square region is separated from Region 1 of section Pattern (1). Figure 8(c) shows that the axial stresses in Region 1 and Region 3 (i.e., σ_1 and σ_3) are very close to each other and both are equal to σ_{c1} during the full loading process. Figure 8(d) shows the stress ratios of section Pattern (4). As Region 1 in this pattern consists of both the central region and the four regions near the flat sides, its average axial stress is always smaller than σ_{c1} and σ_{c2}. The stress ratio of σ_2/σ_{c1} remains almost constant and is slightly larger than 1.0 during the later loading stage. This is reasonable as Region 2 in this pattern includes parts of the regions along the flat sides with low axial stresses (Figure 6), which compensates for the high axial stresses in the rounded corner regions. The non-dimensional parameter β' ($= \sigma_1/\sigma_{c1} - \sigma_1/\sigma_{c2}$) in this pattern, however, does not remain constant but increases with the corner center hoop strain during the later loading stage [Figure 8(d)].

Based on the stress ratio results discussed above, only section Pattern (1) has a nearly constant stress ratio or non-dimensional parameter for each region during the later loading stage. For the other section patterns, although they appear to follow more closely the actual stress distribution, no constant stress ratios or non-dimensional parameters were identified. A constant stress ratio or non-dimensional parameter makes it possible to evaluate the average axial stresses of all regions in a section pattern using the axial stresses from the two equivalent circular sections. For this reason, section Pattern (1) can be regarded as the most desirable pattern for evaluating the axial stress of each region in a square section. Using this section pattern, the non-dimensional parameter β ($= \sigma_2/\sigma_{c1} - \sigma_2/\sigma_{c2}$) is the only parameter that needs to be determined before the average axial stress of the entire square section can be found.

A parametric study using the FE approach was carried out and the aforementioned observations for the stress ratios of section Pattern (1) have been found to be valid for sections covering wide ranges of parametric values. The parameters examined in the parametric study included the sectional width (b = 150, 350, 550, 750, 950, 1100 mm), the corner radius ratio ($2r/b$ = 0.2, 0.3, 0.4, 0.5, 0.6), the stiffness of the FRP jacket ($E_f t_f$ = 40, 60, 80, 100, 120, 140, 160 GPa·mm) and the unconfined concrete strength (f'_{co} = 30, 40, 50, 60 MPa). The extracted axial stress ratios of these columns analyzed in the parametric study are shown in Figure 9. The parametric study results showed that: (1) the average axial stress of Region 1 in section Pattern (1) always equals the axial stress of the equivalent circular section 1 (σ_{c1}) during the later loading stage regardless of the section parameters; (2) the non-dimensional parameter β remains almost constant during the later loading stage but the value depends on the sectional parameters.

5. PROPOSED STRESS-STRAIN MODEL

5.1. General Procedure

The full-range stress-strain curve can be established using an incremental procedure similar to that of the analysis-oriented stress-strain model of Jiang and Teng [6] for FRP-confined concrete in circular columns. Two key assumptions are first made: (1) the analysis-oriented stress-strain model of Jiang and Teng [6] is applicable to the two equivalent circular sections; (2) the corner center hoop strain (ε_h) is taken to be the characteristic hoop strain for both equivalent circular sections. The process is driven by the characteristic hoop strain and needs to follow the steps listed below (a flowchart of the generation process is shown in Figure 10):

1) for a given characteristic hoop strain (ε_h), calculate the confining pressures for the two equivalent circular sections, and then evaluate the corresponding axial stresses (σ_{c1} and σ_{c2}) based entirely on Jiang and Teng's model [6] (including the axial strain-hoop strain relationship for circular columns);
2) calculate the average stresses of concrete in Regions 1 and 2 for the square section using the stress ratio parameters discussed in the preceding section [that is, $\sigma_1 = \alpha\sigma_{c1}$ and $\sigma_2 = \beta/(1/\sigma_{c1} - 1/\sigma_{c2})$];
3) calculate the average stress for the entire square section from $\sigma = (\sigma_1 A_1 + \sigma_2 A_2)/A_g$, where A_1, A_2, A_g are the areas of Region 1, Region 2 and the entire rounded section, respectively;
4) calculate the axial strain of the square section corresponding to the given characteristic hoop strain (ε_h) according to a new axial strain-corner (center) hoop strain relationship; this axial strain together with the average stress from Step 3 determines a point on the stress-strain curve;
5) repeat the above steps until ε_h reaches the FRP hoop rupture strain to generate the entire stress-strain curve.

In order to complete the above procedure, there are three unknown factors that need to be addressed: (1) the stress ratio parameters *α* and *β*; (2) the axial strain-corner hoop strain relationship; and (3) the ultimate condition (the ultimate value of the characteristic hoop strain at jacket rupture). These issues are discussed in the following sub-sections.

5.2. Stress Ratio Parameters

Figure 9 indicates that apart from the initial stage of loading, both *α* and *β* can be approximated by a parabolic curve plus a horizontal line. During the initial stage of loading, the values of both *α* and *β* depend little on the values of relevant geometric or material parameters, although the initial value of *β* depends slightly on these parameters. Based on these observations, both *α* and *β* can be expressed as a piece-wise curve with three stages: a linear function of the hoop strain for Stage 1, a parabolic function for Stage 2, and a horizontal line for Stage 3 (Figure 11). The transition hoop strain values between Stage 1 and Stage 2, namely $\varepsilon_{\alpha 1}$ and $\varepsilon_{\beta 1}$, are almost constant as shown in Figure 8 and both are approximately equal to 0.035%. The transition hoop strain values between Stage 2 and Stage 3, namely, $\varepsilon_{\alpha 2}$ and $\varepsilon_{\beta 2}$ are equal to 0.002 and 0.004, respectively (Figure 11). The equations for *α* and *β* over the full range of loading are thus as follows:

$$\alpha = \begin{cases} \alpha_0 + \varepsilon_h(\alpha_1 - \alpha_0)/\varepsilon_{\alpha 1} & 0 < \varepsilon_h \le \varepsilon_{\alpha 1} \\ a_1\varepsilon_h^2 + b_1\varepsilon_h + c_1 & \varepsilon_{\alpha 1} < \varepsilon_h \le \varepsilon_{\alpha 2} \\ 1.0 & \varepsilon_h > \varepsilon_{\alpha 2} \end{cases} \quad \text{(1a)}$$

$$\beta = \begin{cases} \beta_0 & 0 < \varepsilon_h \le \varepsilon_{\beta 1} \\ a_2\varepsilon_h^2 + b_2\varepsilon_h + c_2 & \varepsilon_{\beta 1} < \varepsilon_h \le \varepsilon_{\beta 2} \\ \beta_{const} & \varepsilon_h > \varepsilon_{\beta 2} \end{cases} \tag{1b}$$

where α_0 and β_0 are the initial stress ratios; α_1 is the value of the stress ratio α at the end of Stage 1; β_{const} is the value of the stress ratio β during the later stage of loading; and (a_1, b_1, c_1) and (a_2, b_2, c_2) are constants to be determined by the condition that: (1) the parabolic curve (Stage 2) connects to the linear line of Stage 1 and the horizontal straight line of Stage 3; and (2) the parabolic curve connects to the horizontal straight line of Stage 3 smoothly (i.e., without a slope change). The connections between the linear line of Stage 1 and the parabolic curve of Stage 2, however, are not smooth. Based on the FE results, α_0 and α_1 can be taken to be 1.1 and 0.8, respectively (Figure 9).

Figure 9 shows that the value of β_{const} falls in the range of 0.2 to 0.5 for a reasonably wide range of parametric values. By analyzing the FE results, β_{const} was found to be related to the corner radius ratio ($2r/b$) and the FRP confinement stiffness ratio of the second equivalent circular section $\rho_{K2} = E_f t_f \big/ \left[\left(f'_{co}/\varepsilon_{co}\right) r\right]$ (Figure 12). It was also found that the value of β_{const} mainly affects the slope of the linear second branch of the stress-strain curve of FRP-confined concrete. A simple regression analysis of the FE results led to the following equation for β_{const}:

$$\beta_{const} \big/ \left[2.45 - 3.00\left(2r/b\right)\right] = 0.0244\ln\left(\rho_{K2}\right) + 0.257 \tag{2}$$

The average value, the coefficient of variation (CoV), and the coefficient of determination value (R^2) of the ratios between the predicted values from Eq. (2) and the FE results are 1.00, 0.023, and 0.990, respectively.

Additionally, based on a regression analysis of the FE results, the initial value of β_0 can be linearly related to the constant value β_{const} for the later stage of loading using the following simple equation as shown in Figure 13:

$$\beta_0 = 0.075\beta_{const} + 0.02 \tag{3}$$

It is worth noting that the above simple equations for α and β are proposed to approximate the stress ratio variations from FE analysis, especially for an early loading stage (with a characteristic hoop strain less than 0.004) (Figure 11). The stress-strain response of FRP-confined concrete during the early loading stage, however, is known to be similar to that of unconfined concrete as FRP confinement has not been fully activated at this stage [11, 24, 51]. As a result, the proposed analytical model can be used with sufficient confidence to predict the full-range stress-strain curve as long as β_{const} is accurately predicted by Eq. (2).

5.3. Axial Strain-Corner Hoop Strain Relationship

In the analysis-oriented stress-strain model of Teng et al. [52], the axial strain-lateral (hoop) strain relationship for FRP-confined concrete in circular columns is described by the following equation:

$$\frac{\varepsilon_c}{\varepsilon_{co}} \Bigg/ \left(1 + 8\frac{f_{lf}}{f'_{co}}\right) = 0.85\left\{\left[1 + 0.75\left(\frac{\varepsilon_h}{\varepsilon_{co}}\right)\right]^{0.7} - \exp\left[-7\left(\frac{\varepsilon_h}{\varepsilon_{co}}\right)\right]\right\} \tag{4}$$

where f_{lf} is the confining pressure provided by the FRP jacket:

$$f_{lf} = \frac{2E_f t_f \varepsilon_h}{D} \tag{5}$$

The FE results revealed that Eq. (4) fails to predict the axial strain-corner hoop strain relationship of an FRP-confined square column which is significantly affected by the sectional shape. Therefore, by introducing the effect of sectional shape on the effectiveness of FRP confinement, the following new expression for the axial strain-corner hoop strain relationship of square columns is proposed:

$$\frac{\varepsilon_c}{\varepsilon_{co}} \Bigg/ \left[1+8\frac{f'_{lf}}{(1.35-0.35k_s)k_s^2 f'_{co}}\right] = 0.85\left\{\left[1+0.75\left(\frac{\varepsilon_h}{\varepsilon_{co}}\right)\right]^{0.7} - \exp\left[-7\left(\frac{\varepsilon_h}{\varepsilon_{co}}\right)\right]\right\} \tag{6}$$

where $k_s \left(= A_1/A_g\right)$ is the ratio between the area of Region 1 and the gross area of the square section to reflect the effect of sectional shape (Figure 6); and f'_{lf} is the effective confining pressure for a square section and can be calculated using the following equation:

$$f'_{lf} = k_s \frac{2E_f t_f \varepsilon_h}{D_{eq}} \tag{7}$$

where D_{eq} is the diameter of the first equivalent circular section (Figure 7). Note that when k_s = 1.0, Eq. (6) reduces to Eq. (4) for circular columns proposed by Teng et al. [52]. Figure 14 shows the performance of Eq. (6) for square sections for which the FE results for the stress ratios are presented in Figure 9.

5.4. Ultimate Condition

In many of the existing tests on FRP-confined rectangular columns, the measured FRP hoop strains are those on the flat sides instead of those on the rounded corners; therefore, the measured FRP rupture strains from these tests are inappropriate for the proposed method. To overcome this problem, the values of the FRP strain efficiency factor k_ε, defined as the ratio between the measured FRP rupture strain from the column test $\varepsilon_{h,rup}$ and that from the coupon test ε_f, were directly estimated from the experimental ultimate axial strains ε_{cu} using the proposed axial strain-corner hoop strain relationship [Eq. (6)] in the present study. A test database consisting of 51 FRP-confined square concrete columns with hardening stress-strain behavior was extracted from a larger test database of square columns from Lin [53]. The detailed parameters of the 51 columns are listed in Table 1. The reason for selecting only specimens with a strongly-hardening stress-strain response lies in the fact that the ultimate points are significantly more scattered for columns with a softening stress-strain behavior and the measured ultimate axial strains differ greatly even for a set of specimens with identical parameters in every aspect [54]. Figure 15 shows that the strain efficiency factor (k_ε) greatly depends on the corner radius ratio ($2r/b$) of the square section. Similar observations have been reported by other researchers (e.g. [14, 35, 55]). As a result, the following equation is proposed for the prediction of the strain efficiency factor of the FRP jacket in square columns:

$$k_\varepsilon = 0.727\left(2r/b\right)^{0.288} \tag{8}$$

6. PERFORMANCE OF THE PROPOSED STRESS-STRAIN MODEL

6.1. Stress-Strain Curve

The experimental results of typical FRP-confined square concrete columns tested by Wang and Wu [14] are used here for the verification of the proposed stress-strain model (Table 1). The predicted results are also compared with those of four existing stress-strain models of the same type, which are from Wang and Restrepo [39], Marques et al. [56] , Lee et al. [31] and Nisticò [41]. In addition, another 20 FRP-confined square concrete columns recently tested by Wang et al. [4], Zeng et al. [57], and Zhu et al. [50] are used to assess the performance of the stress-strain models (Table 2). As these test results were not used in the development of any of the above-mentioned stress-strain models, they provide an independent assessment of the performance of the models. For making predictions for the ultimate condition (i.e., ultimate axial stress and ultimate axial strain) of FRP-confined concrete, Nisticò [41] proposed a predictive equation for the FRP strain efficiency factor on the basis of the experimental FRP rupture strains of the square columns tested by Wang and Wu [14]. Lee et al. [31] specified in their model that the experimental FRP rupture strains should be directly used in calculating the ultimate condition. However, the experimental FRP rupture strains were not reported for some of the columns in Tables 1 and 2, for which Eq. (8) was used instead to calculate the ultimate condition. In Wang and Restrepo's model [39] and Marques et al.'s model [56], the FRP rupture strains obtained from coupon tests (ε_f) were used for the calculation of ultimate condition as specified in their models. For the proposed stress-strain model, Eq. (8) was used for all the columns in Tables 1 and 2.

The predicted stress-strain curves are compared with the test results from Wang and Wu [14] in Figure 16, while the comparisons for the typical test results from Wang et al. [4] and Zhu et al. [50] are shown in Figures 17 and 18, respectively. Figures 16 to 18 show that Nisticò's model [41] significantly underestimates the axial stress in the transition region of the stress-strain curve; the ultimate axial strains of the test columns are also generally underestimated. Lee et al.'s model [31] performs well in predicting the shapes of stress-strain curves, but it generally underestimates the ultimate axial strain. Marques et al.'s model [56] underestimates the axial stresses of the test columns from all the three sources. Wang and Restrepo's model [39] significantly overestimates the axial stresses for most of the columns; it also fails to capture the ultimate axial strains with enough accuracy. The proposed model provides the most accurate predictions for all the test specimens in terms of both the stress-strain curve and the ultimate condition. It is worth noting that the test results from Wang et al. [4] and Zhu et al. [50] were not used in the development of the proposed model. It is also worth noting that some of the specimens tested by Wang et al. [4] and Zhu et al. [50] had relatively large sizes (with a sectional width up to 400 mm) (Table 2), indicating the ability of the proposed model in predicting FRP-confined concrete in large square columns.

The performance of the stress-strain models in predicting the stress-strain curves of FRP-confined concrete in the above test columns was further evaluated using the integral absolute error (IAE) of a stress-strain model. The integral absolute error (IAE) is defined by the following equation [58, 59]:

$$\mathrm{IAE} = \frac{\sum_{i=1}^{m} \left| \mathrm{exp}_i - \mathrm{pred}_i \right|}{\sum_{i=1}^{m} \mathrm{exp}_i} \quad (9)$$

where m is the number of strain points evenly distributed between 0 and the smaller value of the predicted ultimate axial strain and the test ultimate axial strain (set to 20 in the present study); and $\exp_i$ and pred_i are the experimental and predicted stresses at the ith strain point, respectively. The IAE value measures the absolute error of a stress-strain model and indicates the level of agreement between a predicted curve and a test curve. Figure 19 shows the IAE values of the five stress-strain models in predicting the behavior of FRP-confined concrete in the columns tested by Wang and Wu [14], Wang et al. [4] and Zhu et al. [50]. It can be seen that the proposed model has the lowest average value and the lowest standard deviation (~~stdev~~Std.) of the IAE values for the test columns, indicating that the proposed model performs the best among these stress-strain models.

6.2. Ultimate Condition

The ultimate axial stresses and strains of all the test specimens in Tables 1 and 2 were predicted using the five stress-strain models. The performance of each model is assessed herein based on the average absolute error (AAE) calculated by the following equation:

$$\text{AAE} = \frac{\sum_{i=1}^{n} \left| \frac{\exp_i - \text{pred}_i}{\exp_i} \right|}{n} \tag{10}$$

where n is the number of data points; $\exp_i$ and pred_i are the experimental and predicted values, respectively.

Figure 20 shows the AAE values of the five stress-strain models in predicting the ultimate axial stresses and strains of the test columns. It is evident that the proposed model has the lowest AAE value among the five models for both the ultimate axial stress and ultimate axial strain, demonstrating that the proposed model is superior to the existing models of the same type.

7. CONCLUSIONS

This paper has presented an advanced analytical stress-strain model for FRP-confined concrete in square columns based on a new approach. In this new approach, the distribution of axial stress and the interaction between the FRP jacket and the concrete are explicitly accounted for, leading to a stress-strain model which is analogous to analysis-oriented stress-strain models for FRP-confined concrete in circular columns. This new approach is based on a new understanding of the confinement mechanism in square column sections provided by results from a reliable 3D FE approach. Based on the information presented in the paper, the following conclusions can be drawn:

1. The FE results show that the axial stress distribution over an FRP-confined square section is relatively uniform at an early deformation state (before the average axial stress reaches the unconfined concrete strength) but becomes increasingly more non-uniform as the axial deformation further increases.
2. The axial stresses in the four corner regions are much larger than those away from the corners and the axial stresses are the lowest near the mid-widths of the flat sides of the section; the effective confinement area (i.e., the portion of the column cross-sectional area with an average axial stress larger than the unconfined concrete strength) varies as the axial deformation increases.
3. Four section stress patterns were explored to provide an approximate representation of the axial stress distribution. Among the four section patterns, only section Pattern (1), which consists of two diagonal regions and four triangular regions near the four flat sides

respectively, allows a relatively simple representation of stresses over the section: during the later loading stage, the average axial stresses of all regions in this section pattern can be related to the axial stresses from the two equivalent circular sections defined for the section.

4. By introducing the effect of sectional shape on the effectiveness of FRP confinement, an expression for the axial strain-corner hoop strain relationship (Eq. 6) was formulated, which provides accurate predictions for the FE results.
5. The value of FRP strain efficiency factor of the FRP jacket in square columns depends strongly on the corner radius ratio of the square section.
6. The proposed stress-strain model provides accurate predictions for the stress-strain curves of the test columns and performs better than the four existing stress-strain models of the same type. In particular, the proposed model performs better than the other four models in predicting the test results of large-scale columns which have not been used in the development of the present model.

DATA AVAILABILITY STATEMENT

Some or all data, models, or codes that support the findings of this study are available from the corresponding author upon reasonable request.

ACKNOWLEDGEMENTS

The authors are grateful for the financial support received from the National Key R&D Program of China (Project No. 2017YFC0703000), the Research Grants Council of the Hong Kong Special Administrative Region (Project No.: T22-502/18-R), and The Hong Kong Polytechnic University (Project Account Code: 1-BBAG).

REFERENCES

[1] Teng JG, Chen JF, Smith ST, Lam L. FRP: strengthened RC structures2002.

[2] Hollaway LC, Teng JG. Strengthening and Rehabilitation of Civil Infrastructures Using Fibre-Reinforced Polymer (FRP) Composites: Woodhead Publishing, Cambridge, UK, 2008.

[3] Ozbakkaloglu T, Lim JC, Vincent T. FRP-confined concrete in circular sections: Review and assessment of stress–strain models. Engineering Structures. 2013;49:1068-88.

[4] Wang DY, Wang ZY, Smith ST, Yu T. Size effect on axial stress-strain behavior of CFRP-confined square concrete columns. Construction and Building Materials. 2016;118:116-26.

[5] Zeng JJ, Lin G, Teng JG, Li LJ. Behavior of large-scale FRP-confined rectangular RC columns under axial compression. Engineering Structures. 2018;174:629-45.

[6] Jiang T, Teng JG. Analysis-oriented stress–strain models for FRP–confined concrete. Engineering Structures. 2007;29:2968-86.

[7] Teng JG, Jiang T, Lam L, Luo YZ. Refinement of a design-oriented stress–strain model for FRP-confined concrete. Journal of Composites for Construction. 2009;13:269-78.

[8] Lin G, Teng JG. Stress-strain model for FRP-confined concrete in eccentrically loaded circular columns. Journal of Composites for Construction. 2019;23:04019017.

[9] Li P, Wu Y-F, Zhou Y, Xing F. Stress-strain model for FRP-confined concrete subject to arbitrary load path. Composites Part B: Engineering. 2019;163:9-25.

[10] Cao Y, Wu Y-F, Jiang C. Stress-strain relationship of FRP confined concrete columns

under combined axial load and bending moment. Composites Part B: Engineering. 2018;134:207-17.
[11] Lam L, Teng JG. Design-oriented stress-strain model for FRP-confined concrete in rectangular columns. Journal of reinforced plastics and composites. 2003;22:1149-86.
[12] Ozbakkaloglu T, Oehlers DJ. Concrete-filled square and rectangular FRP tubes under axial compression. Journal of Composites for Construction. 2008;12:469-77.
[13] Wu YF, Wei YY. Effect of cross-sectional aspect ratio on the strength of CFRP-confined rectangular concrete columns. Engineering Structures. 2010;32:32-45.
[14] Wang LM, Wu YF. Effect of corner radius on the performance of CFRP-confined square concrete columns: Test. Engineering Structures. 2008;30:493-505.
[15] Eid R, Paultre P. Compressive behavior of FRP-confined reinforced concrete columns. Engineering Structures. 2017;132:518-30.
[16] Isleem HF, Wang DY, Wang ZY. Modeling the axial compressive stress-strain behavior of CFRP-confined rectangular RC columns under monotonic and cyclic loading. Composite Structures. 2018;185:229-40.
[17] Li PD, Sui LL, Xing F, Li M, Zhou YW, Wu YF. Stress–strain relation of FRP-confined predamaged concrete prisms with square sections of different corner radii subjected to monotonic axial compression. Journal of Composites for Construction. 2019;23:04019001.
[18] Jiang JF, Li PD, Nisticò N. Local and global prediction on stress-strain behavior of FRP-confined square concrete sections. Composite Structures. 2019;226:111205.
[19] Fanaradelli T, Rousakis T, Karabinis A. Reinforced concrete columns of square and rectangular section, confined with FRP–Prediction of stress and strain at failure. Composites Part B: Engineering. 2019;174:107046.
[20] de Diego A, Arteaga Á, Fernández J. Strengthening of square concrete columns with composite materials. Investigation on the FRP jacket ultimate strain. Composites Part B: Engineering. 2019;162:454-60.
[21] Rousakis TC, Panagiotakis GD, Archontaki EE, Kostopoulos AK. Prismatic RC columns externally confined with FRP sheets and pre-tensioned basalt fiber ropes under cyclic axial load. Composites Part B: Engineering. 2019;163:96-106.
[22] Masia MJ, Gale TN, Shrive NG. Size effects in axially loaded square-section concrete prisms strengthened using carbon fibre reinforced polymer wrapping. Canadian Journal of Civil Engineering. 2004;31:1-13.
[23] Rousakis TC, Karabinis AI, Kiousis PD. FRP-confined concrete members: Axial compression experiments and plasticity modelling. Engineering Structures. 2007;29:1343-53.
[24] Youssef MN, Feng MQ, Mosallam AS. Stress–strain model for concrete confined by FRP composites. Composites Part B: Engineering. 2007;38:614-28.
[25] Nisticò N. RC square sections confined by FRP: A numerical procedure for predicting stress–strain relationships. Composites Part B: Engineering. 2014;59:238-47.
[26] Pessiki S, Harries KA, Kestner JT, Sause R, Ricles JM. Axial behavior of reinforced concrete columns confined with FRP jackets. Journal of Composites for Construction. 2001;5:237-45.
[27] Ilki A, Kumbasar N. Compressive behaviour of carbon fibre composite jacketed concrete with circular and non-circular cross-sections. Journal of earthquake engineering. 2003;7:381-406.
[28] Tao Z, Yu Q, Zhong YZ. Compressive behaviour of CFRP-confined rectangular concrete columns. Magazine of Concrete Research. 2008;60:735-45.
[29] Abbasnia R, Ziaadiny H. Behavior of concrete prisms confined with FRP composites under axial cyclic compression. Engineering Structures. 2010;32:648-55.
[30] Monti G, Nisticò N. Square and rectangular concrete columns confined by CFRP:

Experimental and numerical investigation. Mechanics of Composite Materials. 2008;44:289.

[31] Lee CS, Hegemier GA, Phillippi DJ. Analytical model for fiber-reinforced polymer-jacketed square concrete columns in axial compression. ACI Structural Journal. 2010;107:208-17.

[32] Lin G, Teng JG. FRP-confined concrete in square columns: an advanced stress-strain model based on a new approach. Proceedings of 4th Asia-Pacific Conference on FRP in Structures (APFIS 2013)2013. p. 11-3.

[33] Mostofinejad D, Ilia E, Mortazavi N. Fibre-reinforced polymer efficiency in square columns with different corner radii. Proceedings of the Institution of Civil Engineers-Structures and Buildings. 2018;171:241-52.

[34] Al-Salloum YA. Influence of edge sharpness on the strength of square concrete columns confined with FRP composite laminates. Composites Part B: Engineering. 2007;38:640-50.

[35] Wang ZY, Wang DY, Smith ST, Lu DG. CFRP-confined square RC columns. I: Experimental investigation. Journal of Composites for Construction. 2012;16:150-60.

[36] Faustino P, Chastre C, Paula R. Design model for square RC columns under compression confined with CFRP. Composites Part B: Engineering. 2014;57:187-98.

[37] Faustino P, Chastre C. Analysis of load–strain models for RC square columns confined with CFRP. Composites Part B: Engineering. 2015;74:23-41.

[38] Restrepol JI, DeVino B. Enhancement of the axial load carrying capacity of reinforced concrete columns by means of fiberglass-epoxy jackets. Proceedings of the 2nd international conference on advanced composite materials in bridges and structures, ACMBS-II, Montreal 19961996.

[39] Wang YC, Restrepo JI. Investigation of concentrically loaded reinforced concrete columns confined with glass fiber-reinforced polymer jackets. Structural Journal. 2001;98:377-85.

[40] Mander JB, Priestley MJN, Park R. Theoretical stress-strain model for confined concrete. Journal of structural engineering. 1988;114:1804-26.

[41] Nisticò N, Monti G. RC square sections confined by FRP: Analytical prediction of peak strength. Composites Part B: Engineering. 2013;45:127-37.

[42] Megalooikonomou KG, Papavasileiou GS. Analytical Stress-Strain Model for FRP-Confined Rectangular RC Columns. Front. Built Environ. 2019;5:39.

[43] Incorporation DSS. Abaqus Analysis User's Manual, Version 6.10. Dassault Systèmes Simulia Incorporation, Providence, Rhode Island, USA; 2010.

[44] Yu T, Teng JG, Wong YL, Dong SL. Finite element modeling of confined concrete-II: Plastic-damage model. Engineering Structures. 2010;32:680-91.

[45] Teng JG, Xiao QG, Yu T, Lam L. Three-dimensional finite element analysis of reinforced concrete columns with FRP and/or steel confinement. Engineering Structures. 2015;97:15-28.

[46] Lin G, Teng JG. Three-dimensional finite-element analysis of FRP-confined circular concrete columns under eccentric loading. Journal of Composites for Construction. 2017;21:04017003.

[47] Mazzucco G, Salomoni VA, Majorana CE, Pellegrino C, Ceccato C. Numerical investigation of concrete columns with external FRP jackets subjected to axial loads. Construction and Building Materials. 2016;111:590-9.

[48] Yu T, Teng JG, Wong YL, Dong SL. Finite element modeling of confined concrete-I: Drucker–Prager type plasticity model. Engineering Structures. 2010;32:665-79.

[49] Zhang YX. Behavior of large-size FRP-jacketed circular and rectangular reinforced concrete columns: The Hong Kong Polytechnic University, 2013.

[50] Zhu JY, Lin G, Teng JG, Chan TM, Zeng JJ, Li LJ. FRP-Confined Square Concrete

Columns with Section Curvilinearization under Axial Compression. Journal of Composites for Construction. 2020;24:04020004.
[51] Harajli MH. Axial stress–strain relationship for FRP confined circular and rectangular concrete columns. Cement and Concrete Composites. 2006;28:938-48.
[52] Teng JG, Huang YL, Lam L, Ye LP. Theoretical model for fiber-reinforced polymer-confined concrete. Journal of Composites for Construction. 2007;11:201-10.
[53] Lin G. Seismic performance of FRP-confined RC columns: stress-strain models and numerical simulation. 2016.
[54] Wei YY, Wu YF. Unified stress–strain model of concrete for FRP-confined columns. Construction and Building Materials. 2012;26:381-92.
[55] Pellegrino C, Modena C. Analytical model for FRP confinement of concrete columns with and without internal steel reinforcement. Journal of Composites for Construction. 2010;14:693-705.
[56] Marques SPC, Marques DCdSC, Lins da Silva J, Cavalcante MAA. Model for analysis of short columns of concrete confined by fiber-reinforced polymer. Journal of Composites for Construction. 2004;8:332-40.
[57] Zeng JJ, Guo YC, Gao WY, Li JZ, Xie JH. Behavior of partially and fully FRP-confined circularized square columns under axial compression. Construction and Building Materials. 2017;152:319-32.
[58] Girgin ZC, Arioglu N, Arioglu E. Evaluation of strength criteria for very-high-strength concretes under triaxial compression. ACI Structural Journal. 2007;104:278.
[59] Wu YF, Jiang C. Effect of load eccentricity on the stress-strain relationship of FRP-confined concrete columns. Composite structures. 2013;98:228-41.

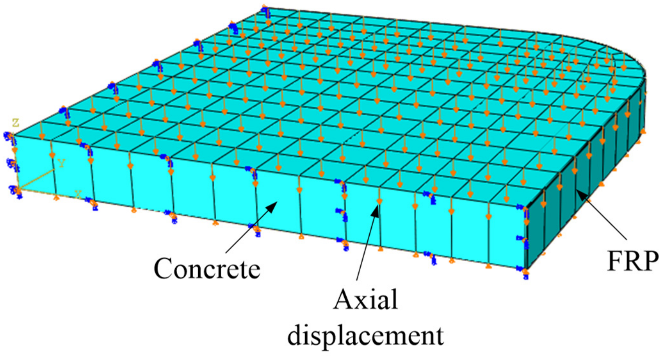

Figure 1 FE slice model of a quarter of a square column

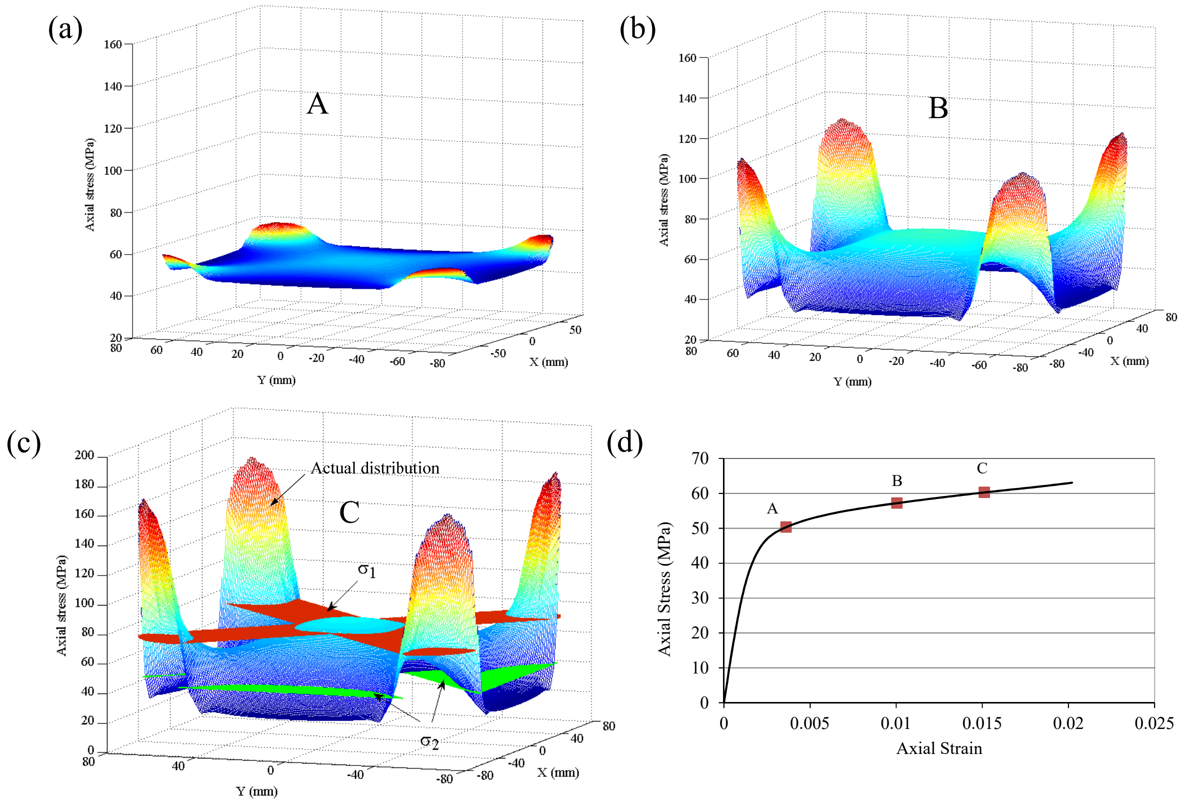

Figure 2 Axial stress distributions over a square section at: (a) State A; (b) State B; (c) State C; (d) average axial stress-axial strain curve

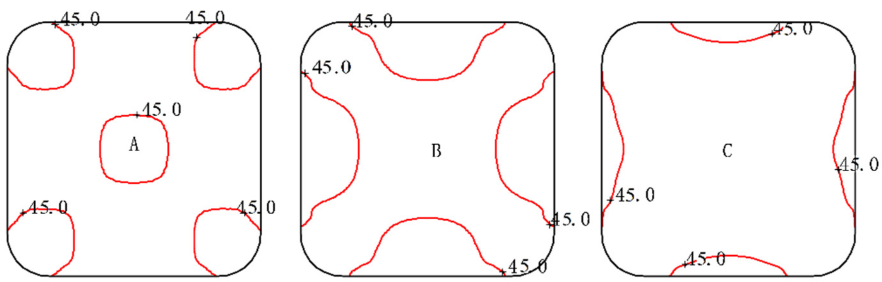

Figure 3 Contour plots of axial stress distribution at different deformation states

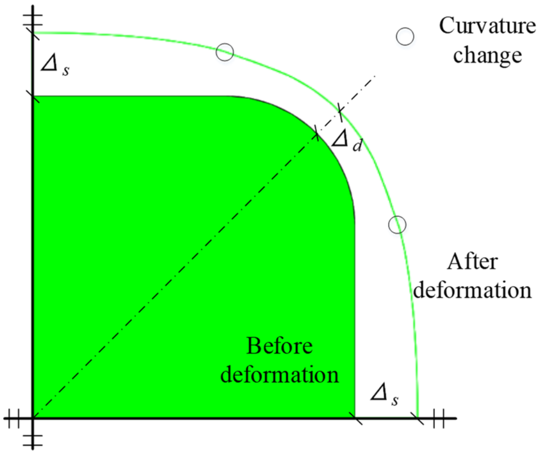

Figure 4 Lateral deformation at State C (Scale factor = 10)

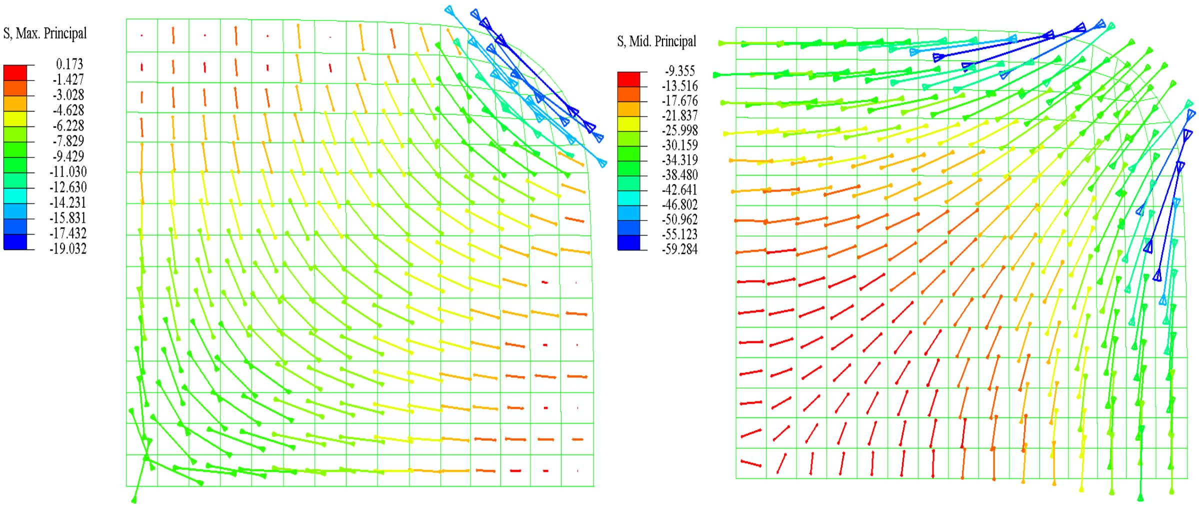

(a) Maximum principal stress (b) Middle principal stress

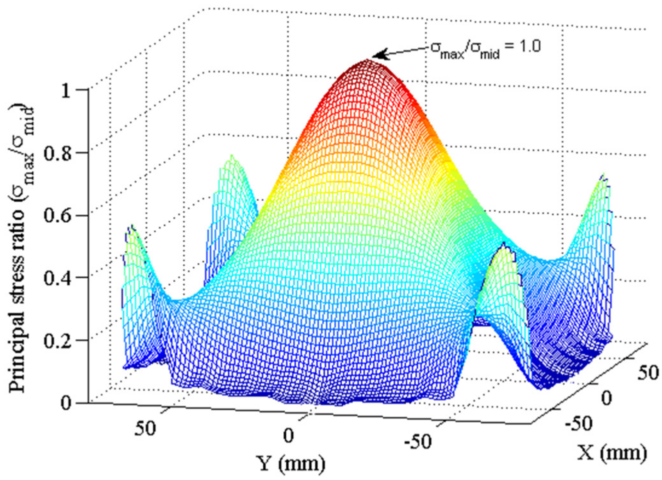

(c) Distribution of principal stress ratio ($\sigma_{max}/\sigma_{mid}$)

Figure 5 Distributions of principal stresses over the square section at State C

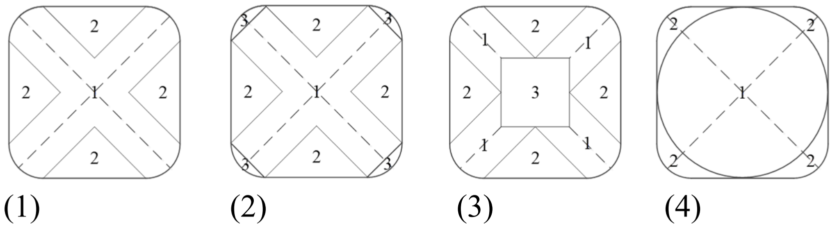

Figure 6 Four patterns of section division

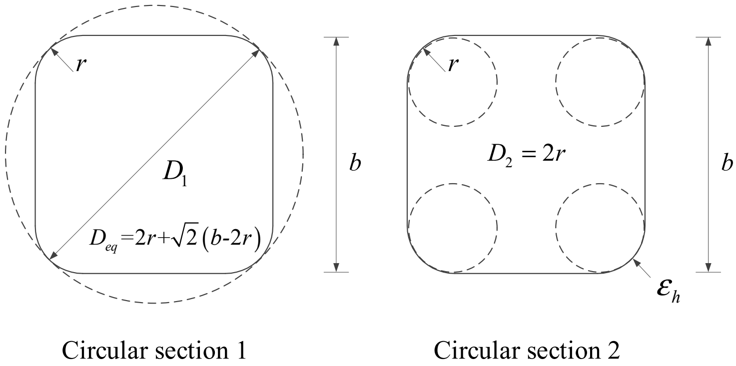

Figure 7 Equivalent circular sections

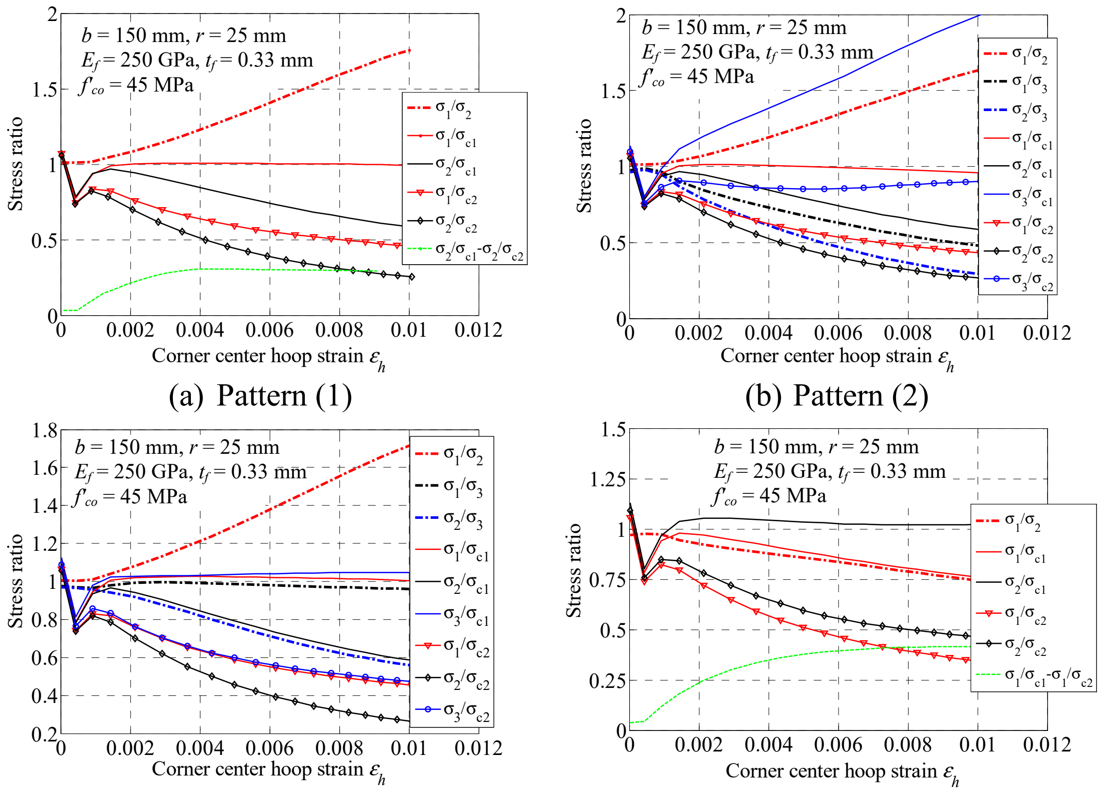

(a) Pattern (1) (b) Pattern (2)

(c) Pattern (3) (d) Pattern (4)

Figure 8 Stress ratios for each section pattern

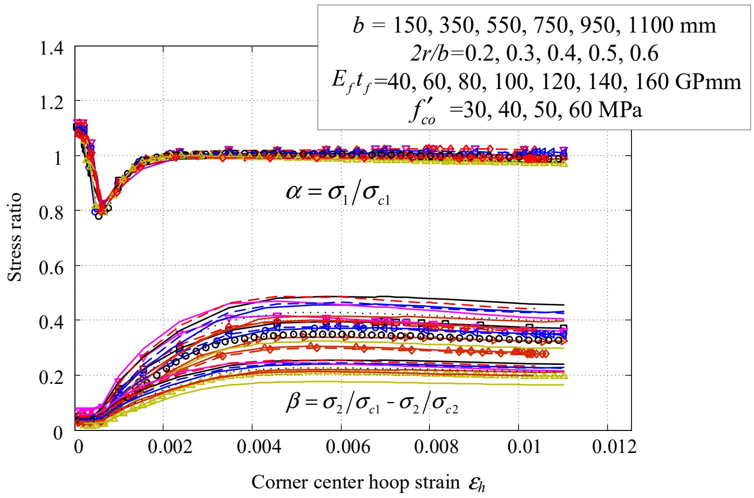

Figure 9 Effect of section parameters on stress ratios for section Pattern (1)

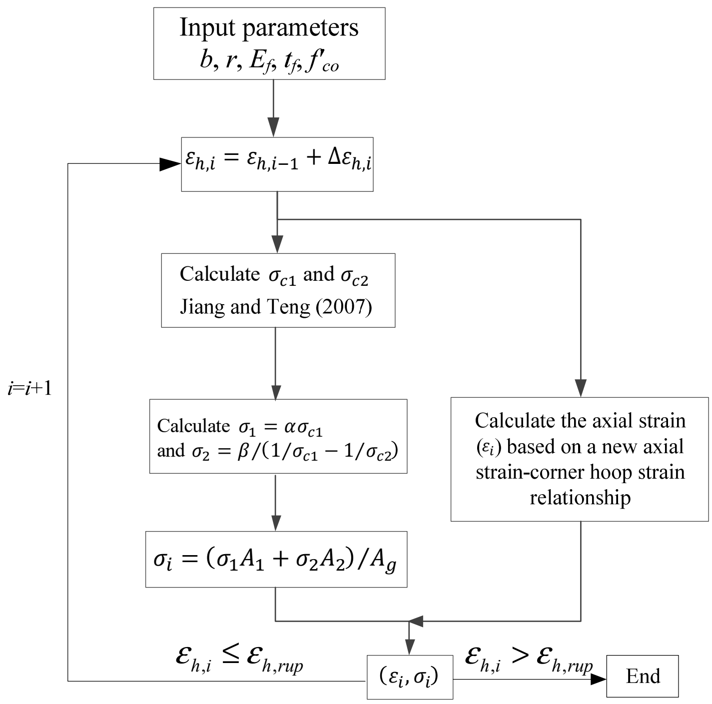

Figure 10 Flowchart for generating stress-strain curves of FRP-confined concrete in square columns

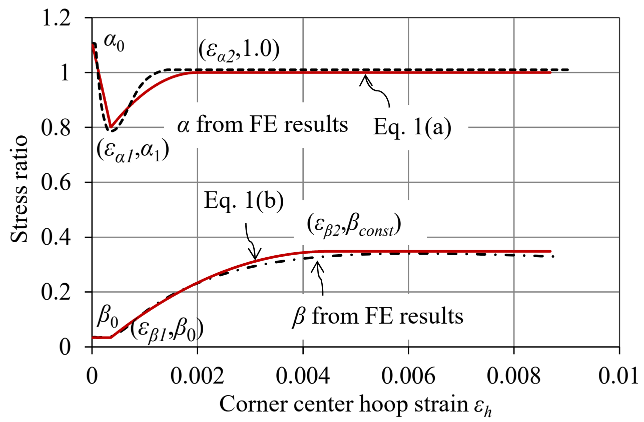

Figure 11 Approximations for the two stress ratio parameters

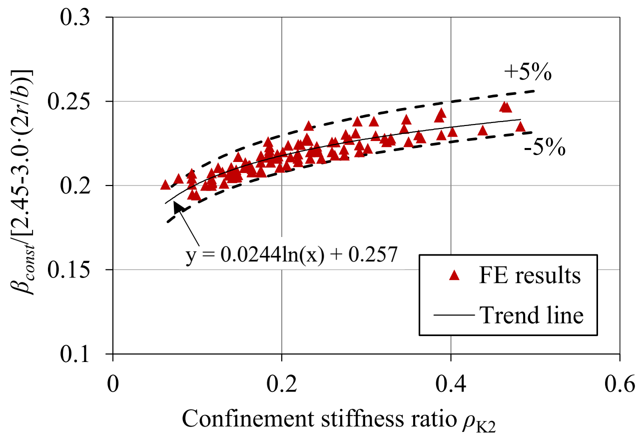

Figure 12 Stress ratio parameter β during the later stage of loading

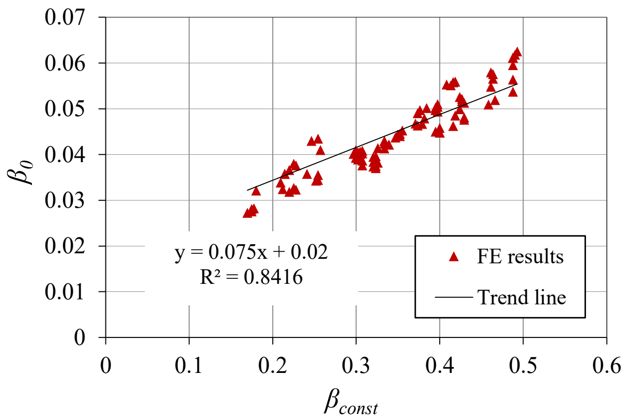

Figure 13 Relationship between β_{const} and β_0 from FE results

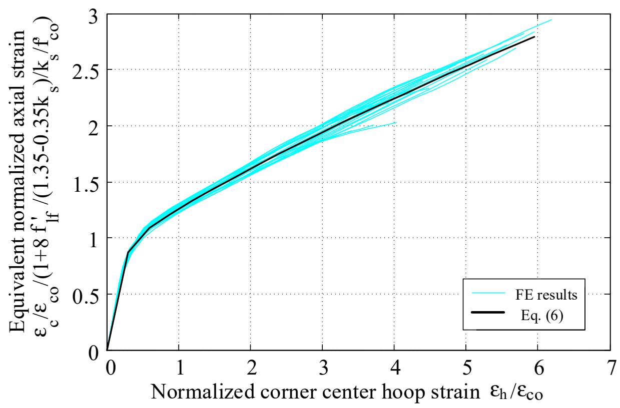

Figure 14 Axial strain-corner hoop strain relationship for square columns

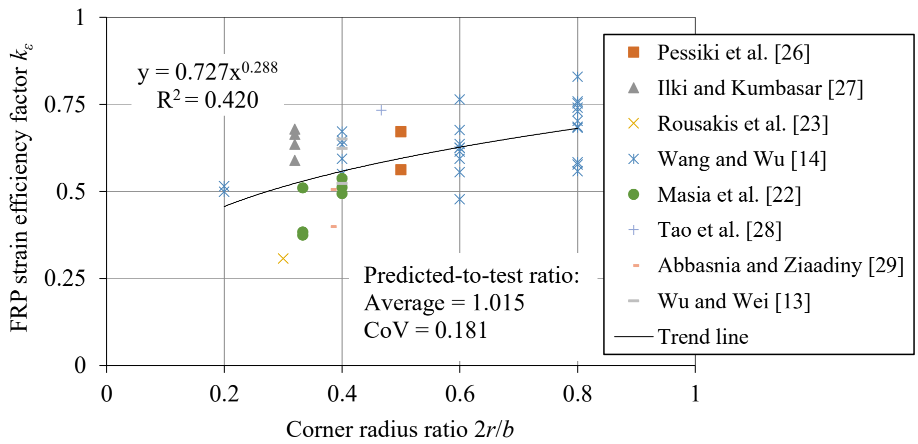

Figure 15 Dependence of FRP strain efficiency factor on corner radius ratio

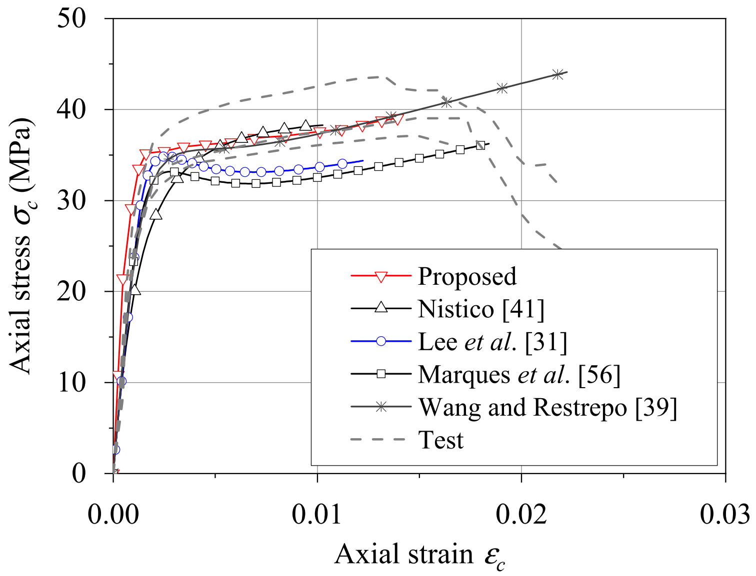

(a) Specimen C30r30F1

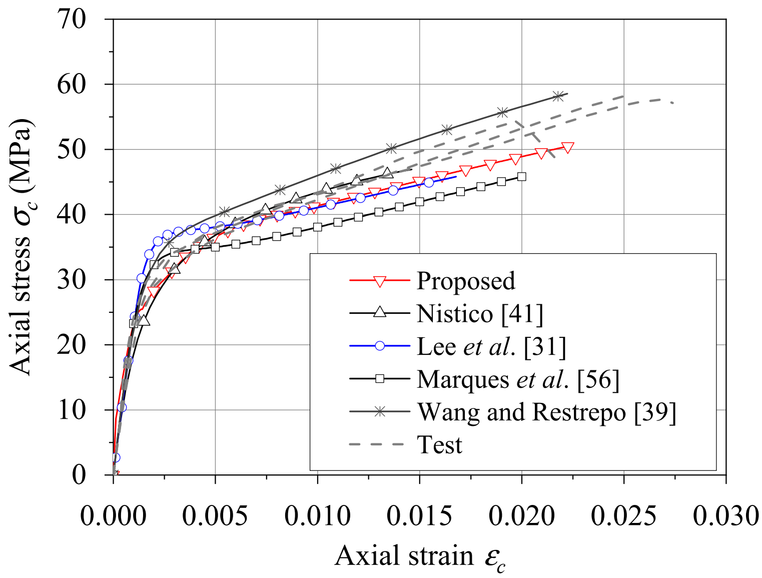

(b) Specimen C30r30F2

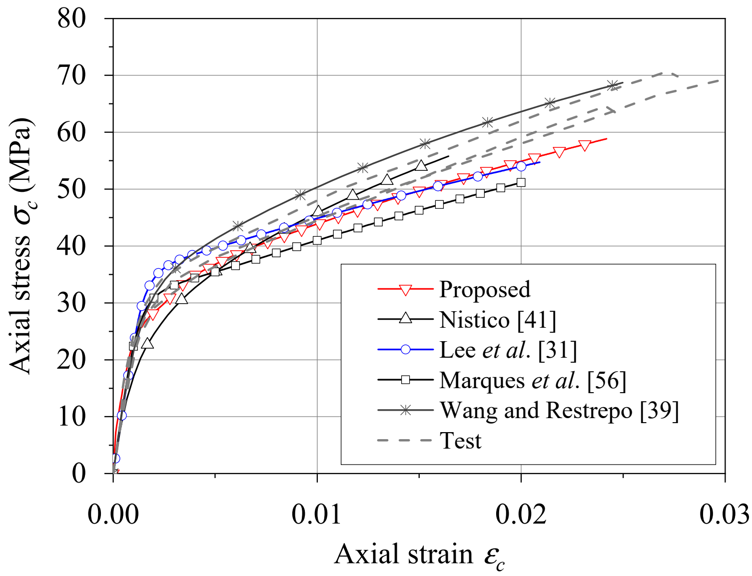

(c) Specimen C30r45F2

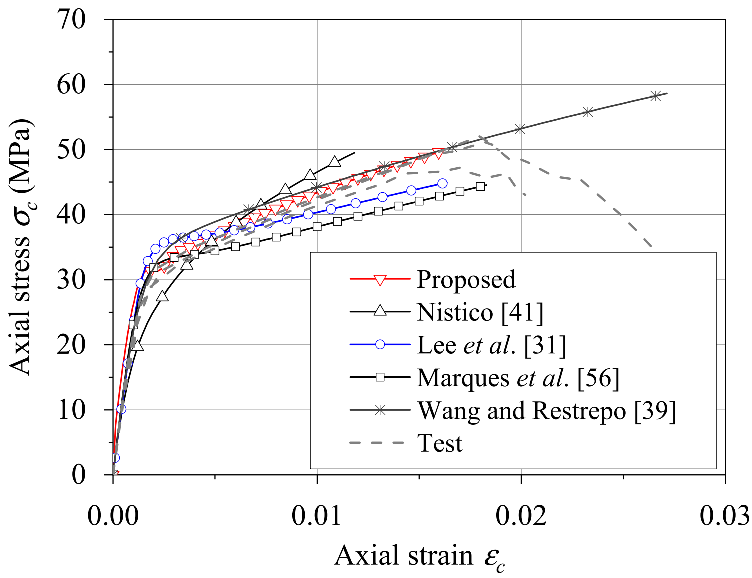

(d) Specimen C30r60F1

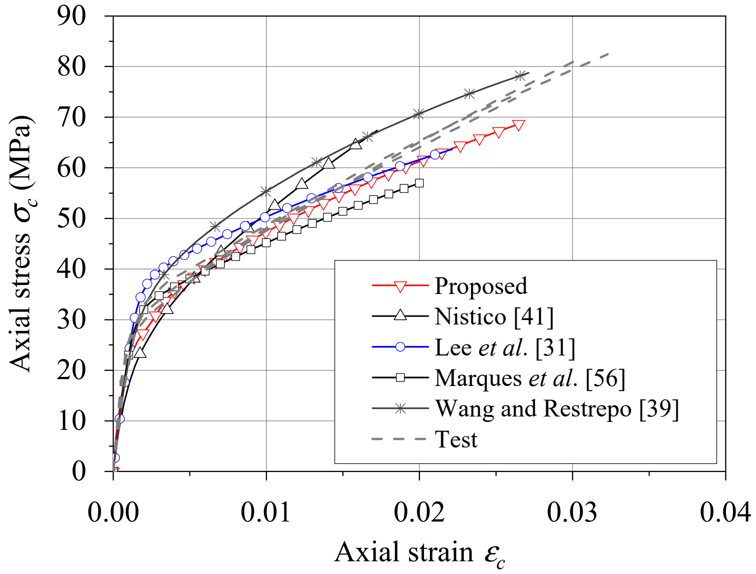

(e) Specimen C30r60F2

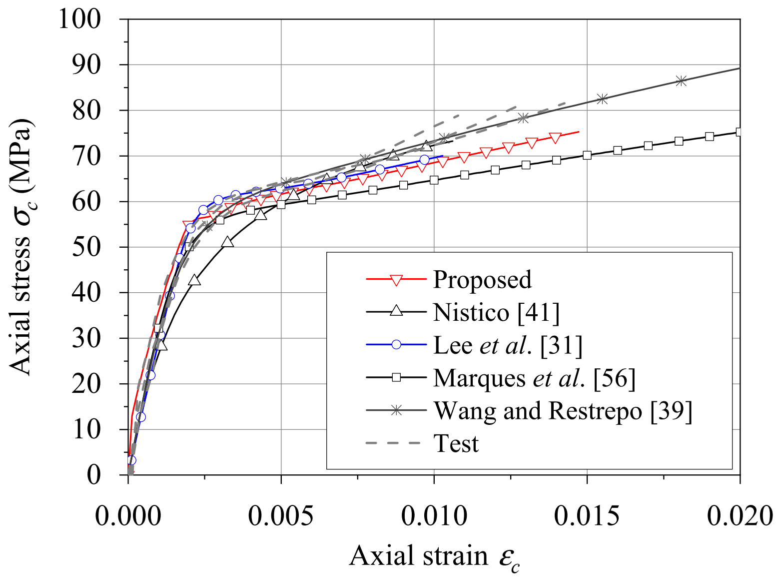

(f) Specimen C50r45F2

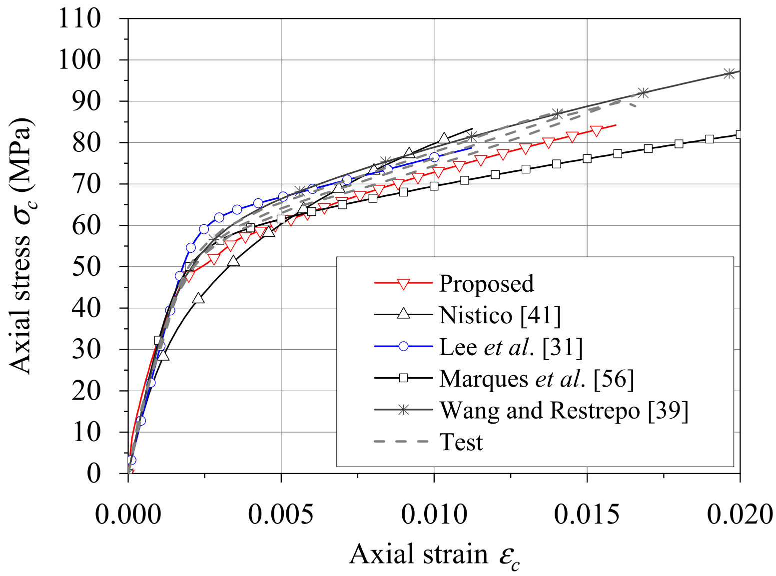

(g) Specimen C50r60F2

Figure 16 Performance of stress-strain models for columns tested by Wang and Wu [14]

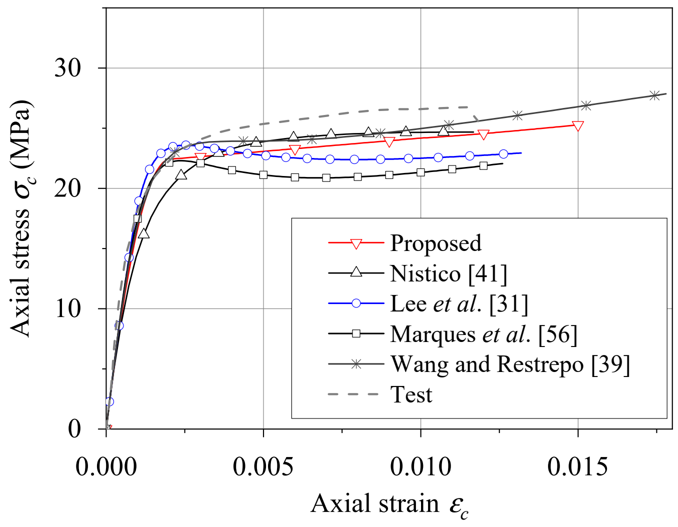

(a) Specimen P350L2

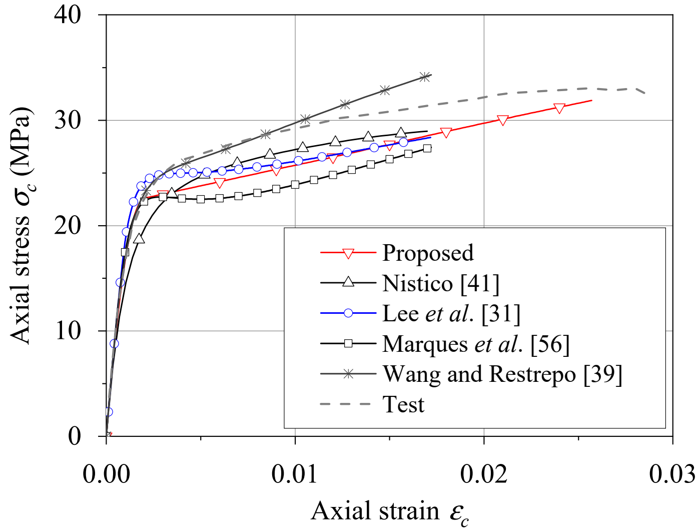

(b) Specimen P350L4

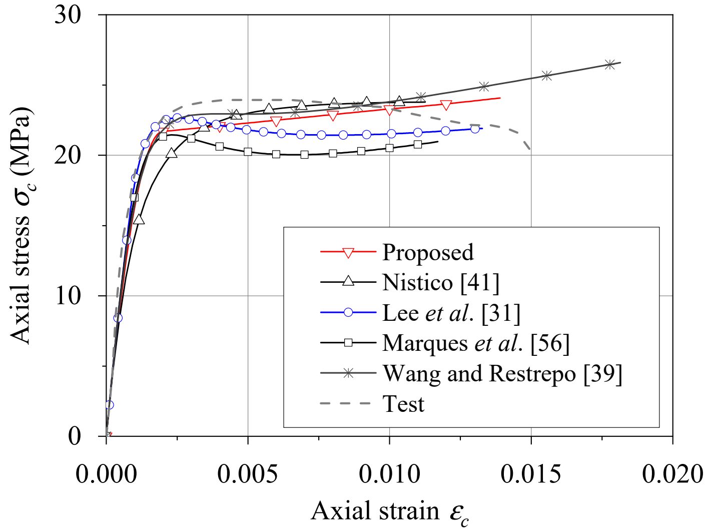

(c) Specimen P400L2

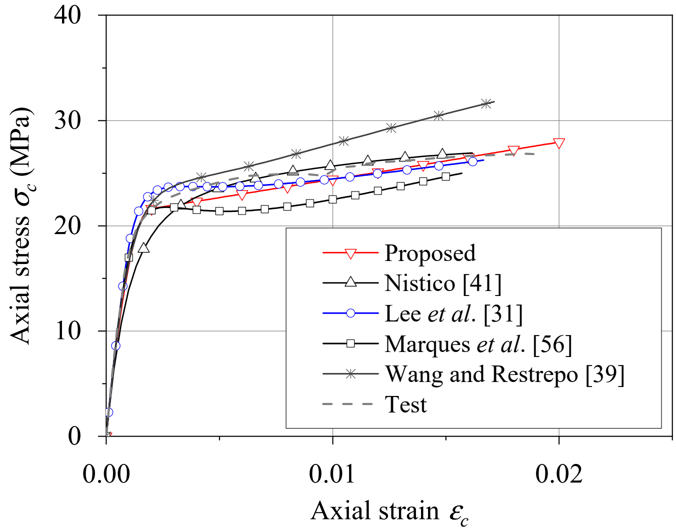

(d) Specimen P400L4

Figure 17 Performance of stress-strain models for columns tested by Wang *et al*. [4]

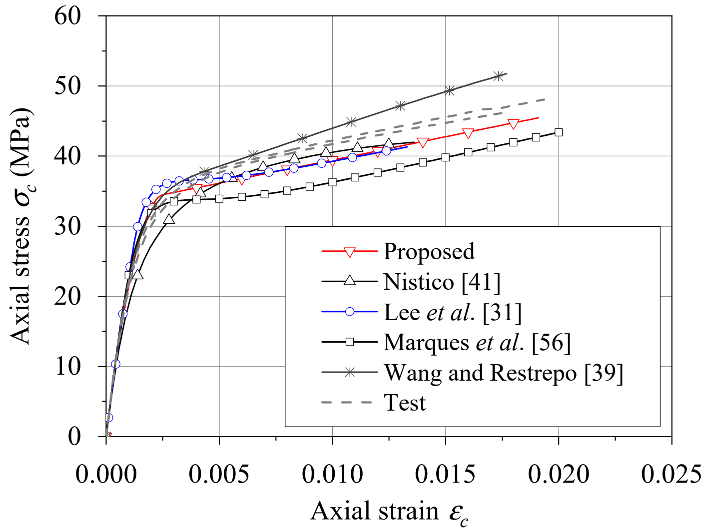

(a) Specimen 2-sq-1/2

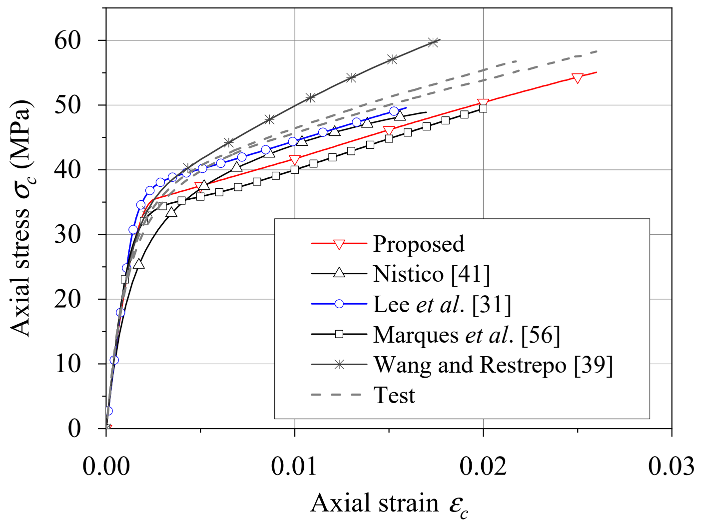

(b) Specimen 3-sq-1/2

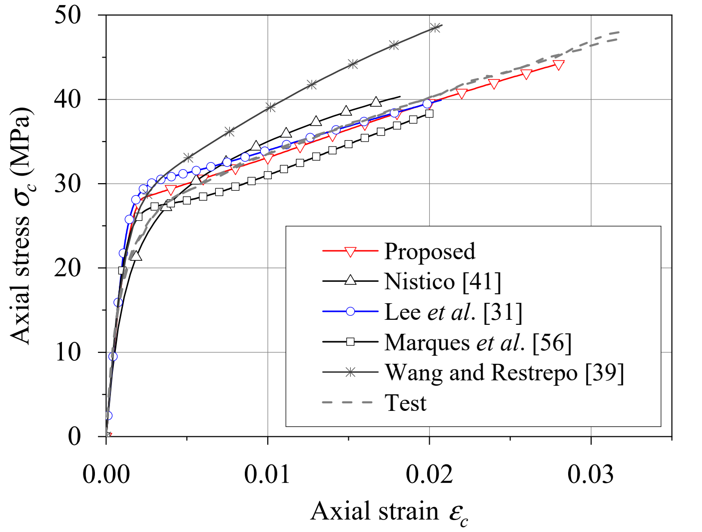

(c) Specimen 4-sq-1/2

Figure 18 Performance of stress-strain models for columns tested by Zhu *et al*. [50]

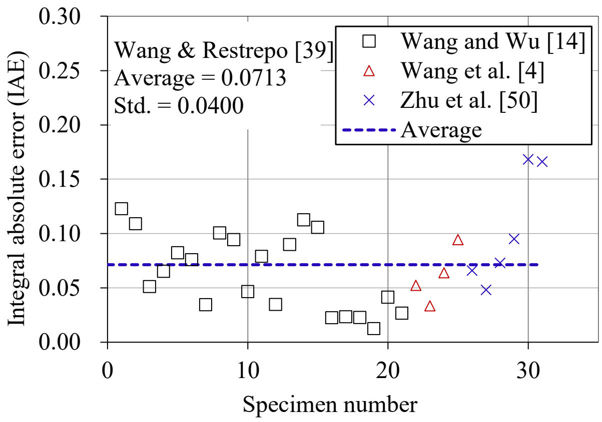

(a) Wang and Restrepo [39]

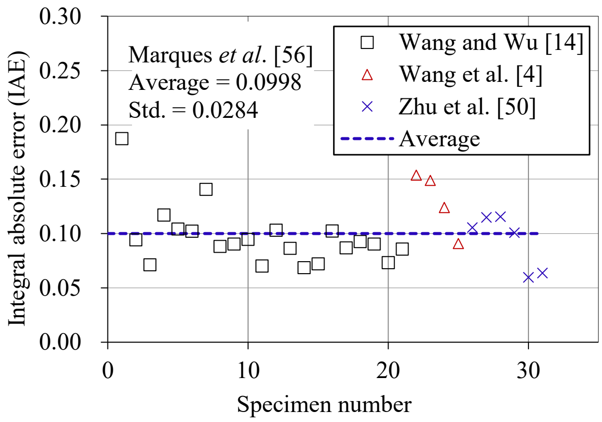

(b) Marques *et al*. [56]

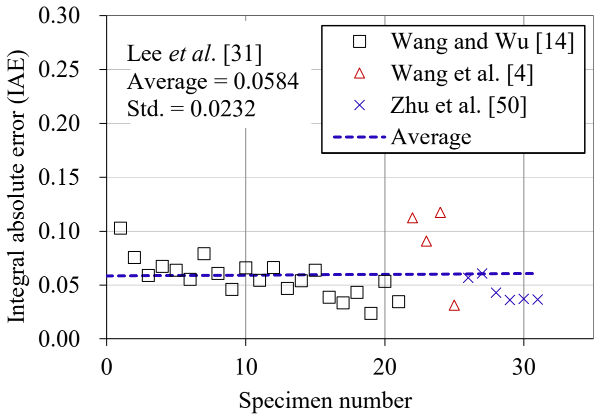

(c) Lee *et al*. [31]

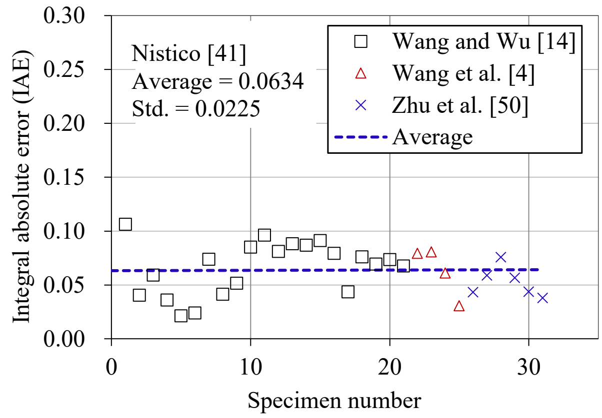

(d) Nistico [41]

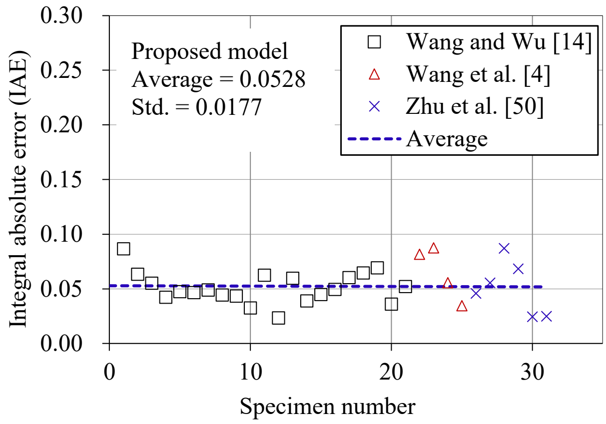

(e) Proposed model

Figure 19 Errors of stress-strain models in predicting experimental stress-strain curves

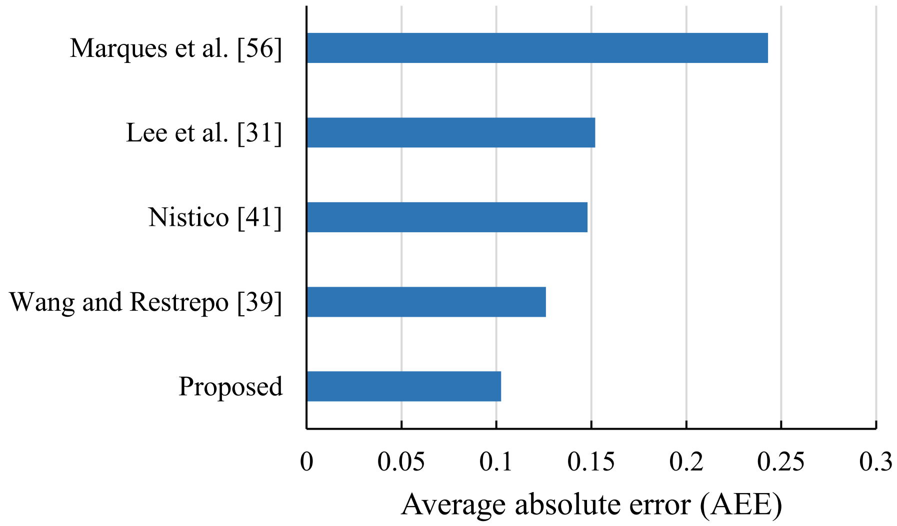

(a) Ultimate axial stress

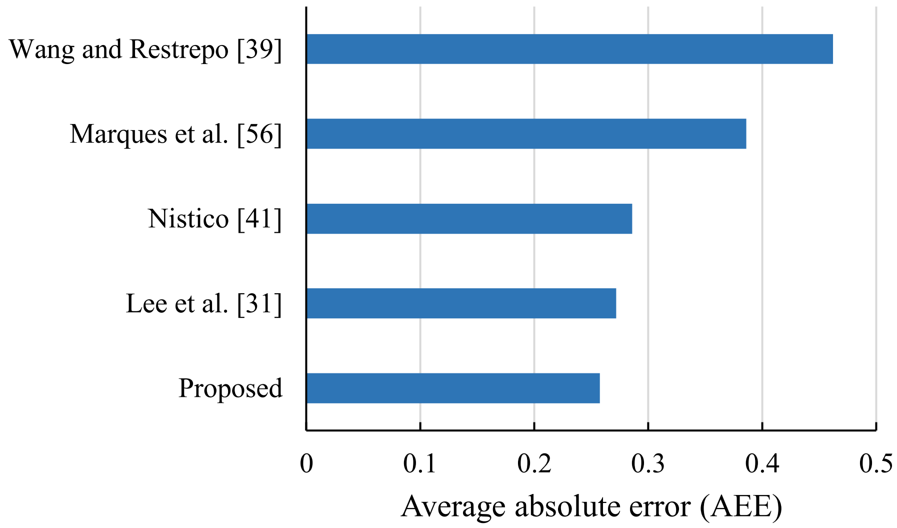

(b) Ultimate axial strain

Figure 20 Errors of stress-strain models in predicting the ultimate condition of FRP-confined concrete in the test columns

Declaration of interests

The authors declare that they have no known competing financial interests or personal relationships that could have appeared to influence the work reported in this paper.

Credit Author Statement

G. Lin: Methodology, Investigation, Formal analysis, Visualization, Writing - original draft
J.G. Teng: Conceptualization, Methodology, Supervision, Visualization, Writing - Review & Editing, Funding acquisition